CHAPTER III

DYNAMIC MODELING OF A WHEELED MOBILE ROBOT

The motion of a mechanical system is related through a set of dynamic equations, and the forces or torques the system is subjected to. The dynamics of a mechanical system has been discusses in a numerous scholarly literatures related to engineering mechanics and analytical mechanics. The study of this subject is important due to the problem of the control of the system, which is in contact with its environment. Indeed, for a model-based controller, the synthesis of the controller of such system depends heavily on the mathematical model of the physical structure of the system, which is intrinsically nonlinear. Thus, the goal here is to develop a model that can describe the dynamics of the system as close to the real system so that we can have a better chance to develop a controller for the system that is effective in real-world situation. In the case of a WMR, the contact with the environment occurs at the contact point between the wheel outer surface and the ground surface. The interaction between these two surfaces has a significant influence over the dynamic motion of the system, and hence, need to be properly modeled.

In general, there are two major methods for deriving the dynamic equations of mechanical systems namely Newton's method that is directly related to Newton's 2nd law and Lagrange's method that has its root in the classical work of d'Alembert and Lagrange on analytical mechanics. The main difference between the two methods is in dealing with constraint equations. While Newton's method treats each rigid body separately and

explicitly model the constraints through the reactive force required to enforce them, Lagrange's provides systematic procedures for eliminating the constraints from the dynamic equations, typically yielding simpler system equations. Thus, it is not surprising that the majority of the conventional WMR models we found in the literature were developed using Lagrange's as a method of choice.

In this chapter, we first describe system constraints and formulate the dynamic equation of the conventional WMR using Lagrange's method. While the parts of the generalized formulation are not new and were previously explored by several researchers (Conceicao et al. 2007, Dongbin et. al 2007, Eghtesad & Necsulescu 2006, Liyong & Wei 2007, Salerno & Angeles 2007), the formulation is needed and serves as an important platform to combine the slip dynamics with that of the WMR. We then develop a detailed model for a two-WMR (i.e., two differential driving wheels) that is one of the most commonly available WMRs using the generalized formulation. Following that is the detailed discussion on the formulation of the dynamics model of a two-WMR with the inclusion of slips. This model is first developed using Lagrange's, allowing us to present the model in the standard form. In order to ensure model consistency, we present the derivation of dynamic equations using Newton's method. We list down all the variables with their definitions to help in the modeling process of the WMR system in the following table.

Table 3.1: Variables used in the model formulation and their definitions

$\{X, Y\}$	The coordinate system for the inertial frame
$\{x, y\}$	The coordinate system for the WMR reference frame

P_o	the origin of the WMR reference frame with coordinate $\{x_o, y_o\}$
P_c	the center of mass of the WMR with coordinate $\{x_c, y_c\}$
P_l	the virtual reference point (the look-ahead point) attached to the WMR with coordinate $\{x_l, y_l\}$
φ	the angular displacement of WMR
θ_1, θ_2	the angular displacement of the driving wheels
ξ_1, ξ_2	the longitudinal displacement of the driving wheels due to slips
η_1, η_2	the lateral displacement of the driving wheels due to slips
m_r	the effective mass of the WMR without the driving wheels and the motors
m_w	the effective mass of the driving wheels and the motors
I_{rz}	the moment of inertia of the WMR without the driving wheels and the motors taken at the center of mass about the vertical axis.
I_{wz}	the moment of inertia of the driving wheels and the motors about the vertical axis
I_{wy}	the moment of inertia of the driving wheels and the motors about the wheel axis (the WMR lateral axis)
l	the distance between the point P_c and P_l
d	the distance between the point P_o and P_c
b	the distance between the driving wheel and the origin of axis of symmetry of the robot reference frame
a	the length of the WMR platform parallel to it *x*-axis
h	the height of the WMR platform in the direction of the *z*-axis
r	the radius of the driving wheels

System constraints

Mechanical systems can be classified into linear and nonlinear systems. Nonlinear systems can be further classified into holonomic and nonholonomic systems. A wheeled mobile robot is an example of mechanical system that falls under the latter category. Holonomy and nonholonomy are fundamental concepts that describe the constraints of the systems, which play the essential part in governing the motion of those systems.

In the following we define some terms related to the discussion. These definitions are taken from (Rosenberg 1977, Sarkar 1993).

Lagrangian coordinates: Set of coordinates, Q, (not necessarily a minimal set) that are required to distinctively specify the configuration of the system.

If the number of Lagrangian coordinates is more than the number of degree of freedom (DOF) of a system, N, then we may assign N of the Lagrangian coordinates as *primary coordinates*. The remaining coordinates are called *secondary coordinates*. In classical mechanics, the primary coordinates are called *generalized coordinates.*

Catastatic and acatastatic constraints: The general form of equality constraints considered in classical mechanics is given as,

$$\sum_{s=1}^{n} A_{rs} dq_s + A_r dt = 0 \quad , r \in \{1,2, \dots, m\}$$

in which $q = [q_1 \;\; q_2 \;\; \dots \;\; q_n]^T$ are the generalized coordinates of the dynamic systems, t is the time, and A_{rs} and A_r are at least one piecewise differentiable function of q. These m linear differential forms are called *Pfaffian* form. If A_r is zero, and the set of constraint is called catastatic and the resulting dynamic system is called catastatic system. Otherwise the constraint is called acatastatic.

Holonomic constraint: Any constraint of the form,

$$f_c(q,t) = 0 \tag{3.1}$$

where q is the generalized coordinate of the system and t is the time.

Nonholonomic constraint: Any constraint that cannot be reduced (i.e., non-integrable) to form Eq. (3.1)

In general cases of mechanical systems, nonholonomic constraint can be written as,

$$f_c(q,\dot{q},t) = 0 \tag{3.2}$$

A holonomic constraint as in Eq. (3.1) reduces the degree of freedom (DOF) of the system. For instance if there is m number of holonomic constraints with n number of generalized coordinates q_j, where $j \in \{1,2,\dots,n\}$, the number of independent coordinates are $n-m$, which is the DOF of the system. Thus, $n-m$ number of coordinates is needed to describe the system configuration and $n-m$ number of inputs is required to drive the system.

On the other hand, for nonholonomic constrained system, there are two types of DOF, namely the DOF in the small (for infinitesimal displacements), which is $n-m$ and DOF in the large (for finite displacements). The DOF in the large is the same as the minimum number of independent coordinates required to specify the configuration of the system. Nonholonomic system has fewer DOF in the small than that in the large.

For a nonholonomic WMR system, Eq. (3.2) can be further simplified to,

$$f_c(q,\dot{q}) = 0 \tag{3.3}$$

to form a nonholomic kinematic constraint of the system. Examples of such nonholonomic constraint equalities are the rolling of the wheels and the side wise motion of the WMR. Eq. (3.3) represents a velocity-level constraint of the system at the given configuration. The non-integrable nature of the constraint does not necessarily reduce the

number of generalized coordinates. Consequently, there arises possibility to steer the system using less number of inputs (Kurfess 2005, Melchiorri & Tornambe 1996).

Dynamic model of a general nonholonomic WMR

Let us consider a nonholonomic system whose vector of generalized coordinates, and vector of longitudinal and angular velocities are defined as $q \in \Re^{n\times 1}$ and $\dot{q} \in \Re^{n\times 1}$, respectively. If the system is subjected to a set of constraint forces given by Q_k, where $k = 1,2,\dots,n-m$, then there will be m nonholonomic constraint equations that must be explicitly satisfied by the system. We can write the constraint equations in *Pfaffian* form (Eq. (3.3)) as follows,

$$A(q)\dot{q} = 0,\ c \in \{1,2,\dots,m\} \tag{3.4}$$

where $A(q) = \frac{\partial f_c}{\partial q} \in \Re^{m\times n}$ is the *Jacobian* of Eq. (3.3) and is called the constraint matrix. It is full rank matrix everywhere. By using the Lagrange's method, when the WMR is subjected to the nonholonomic kinematic constraints of the form Eq. (3.4), the *Lagrangian* equation of motion can be written as follows,

$$\frac{d}{dt}\left(\frac{\partial L}{\partial \dot{q}_j}\right) - \frac{\partial L}{\partial q_j} = u_j + A(q)^T\lambda_k,\ j \in \{1,2,\dots,n\}, k \in \{1,2,\dots,n-m\} \tag{3.5}$$

where, $L = T - P$ is the *Lagrangian* function. T is the total kinetic energy and P is the total potential energy of the system. u_j is the generalized force corresponding to the generalized coordinate q_j. λ_k is a vector of *Lagrange* multiplier that accounts for the constraint induced force $A(q)^T\lambda_k$. By solving the *Lagrangian*, we can formulate the general dynamic equation of the system as follows,

$$M(q)\ddot{q} + C(q,\dot{q})\dot{q} = B(q)u + A^T\lambda \tag{3.6}$$

where $M(q) \in \Re^{n\times n}$ is called the inertia matrix of the system. $C(q,\dot{q}) \in \Re^{n\times 1}$ is the centrifugal and Coriolis matrix. $B(q) \in \Re^{n\times(n-m)}$ and $u \in \Re^{(n-m)\times 1}$ are the input transformation matrix and input vector, respectively. $\lambda \in \Re^{m\times 1}$ is a vector of *Lagrange* multipliers and $A(q) \in \Re^{m\times n}$ is a constraint matrix that is *adjoined* to the dynamic equation. Several properties of the dynamic equation, Eq. (3.6) can be observed (Das & Kar 2006),

P1: The inertia matrix $M(q)$ is symmetric and positive definite.

P2: The matrix $(\dot{M} - 2C)$ is skew symmetric resulting in the following characteristic, $q^T(\dot{M} - 2C)q = 0$ for all $q \in \Re^n$

For the WMR shown in Fig. 3,1, the generalized system coordinates are given as,

$$q = [x_c, y_c, \varphi, \theta_1, \theta_2, \theta_3, \dots, \theta_{n-1}, \theta_n]^T \tag{3.7}$$

where $(x_c,\ y_c)$ is the coordinate of the reference point on the WMR platform, φ is the platform orientation with respect to an inertial frame $\{x_I, y_I\}$ and $\theta_i, i = 1,2,\dots,n$ are the wheel angular displacements.

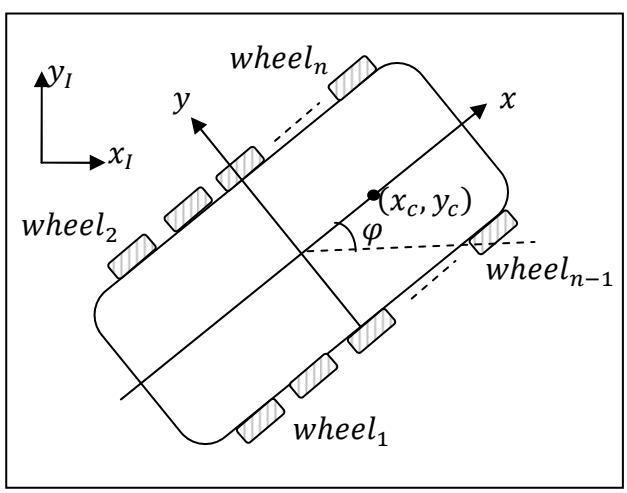

Fig. 3.1: Generalized nonholonomic WMR platform

In many conventional WMR systems, the constraint equations in Eq. (3.4) are defined under the assumption that the wheel rolls without longitudinal slip and there is no lateral slip. That means, the longitudinal velocity of the WMR is governed by the linear velocity of the wheel that is solely defined using the wheel angular velocity and there is no velocity along the lateral direction. Hence, if slip occurs, these assumptions are clearly violated.

In this dissertation, we argue that the modeling of the WMR that is based on the assumptions of wheel pure rolling and zero lateral slipping (for WMR with unicycle type of wheel) in a real practical situation is rather unrealistic. Our solution is to relax the assumptions by introducing new states due to wheel slip.

As shown in Fig. 3.2, we introduce ζ_i and η_i to represent the longitudinal slip displacement and the lateral slip displacement, respectively, for the *i*-th wheel of the WMR. The wheels are rigidly connected to the WMR body as shown in Fig. 3.1.

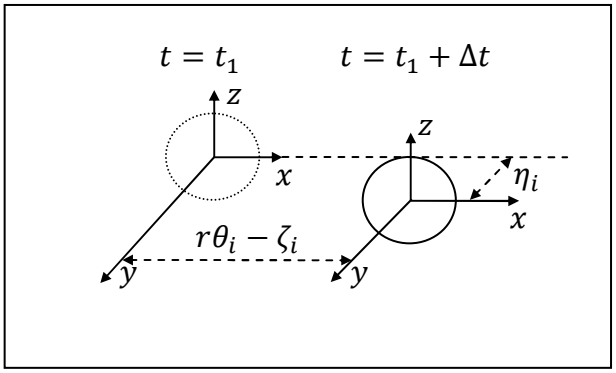

Fig. 3.2: System motion contributed by wheel's rolling and both longitudinal and lateral slips on a planar surface

We can write a new state, ρ_i to represent the total longitudinal displacement of the i-th wheel as,

$$\rho_i = r\theta_i - \zeta_i \tag{3.8}$$

The new coordinate system allows us to describe the motion of the system in the presence of slip. We then define $S(q) \in \Re^{n\times(n-m)}$ to be a full rank matrix formed by a set of smooth and linearly independent vector fields, spanning the null space of $A(q)$. Thus, the result of multiplication of these matrices can be written as follows,

$$S(q)^T A(q)^T = 0 \tag{3.9}$$

It is then possible to find a set of vector of time functions, that is, for all t,

$$\nu(t) \in \Re^{(n-m)\times 1} \tag{3.10}$$

so as,

$$\dot{q}(t) = S(q)\nu(t) \tag{3.11}$$

We can use matrix $S(q)$ from Eq. (3.9) to eliminate the *Lagrange* multipliers in general dynamic equation, Eq. (3.6). We further differentiate Eq. (3.11), to get the state acceleration as follows,

$$\ddot{q}(t) = \dot{S}(q)\nu(t) + S(q)\dot{\nu}(t) \tag{3.12}$$

By placing Eq. (3.11) and Eq. (3.12) into the dynamic equation, Eq. (3.6), we obtain,

$$S^T MS\dot{\nu} + S^T M\dot{S}\nu + S^T CS\nu = S^T Bu \tag{3.13}$$

Eq. (3.13) describes the dynamics of the nonholonomic WMR system in a new set of local coordinates ν, such that matrix $S(q)$ projects the velocities, ν in the WMR base coordinate to velocities in Cartesian coordinate, $\dot{q}$. Therefore the properties of the original dynamics hold for the new set of coordinates that is,

P3: The matrix $(S^T MS)$ is symmetric and positive definite

P4: The matrix$(S^T\dot{M}S) - 2(S^T M\dot{S})$ is skew-symmetric.

We can rearrange Eq. (3.13) to form,

$$\dot{v}(t) = (S^T MS)^{-1} S^T\left(-M\dot{S}v - Cv - Bu\right) \tag{3.14}$$

$\dot{v}(t)$ is the acceleration of vector time function defined in Eq. (3.10). Based on the equation Eq. (3.14), we can develop a suitable model-based controller for the WMR system.

Detailed modeling of a two-wheeled nonholonomic mobile robot

Now we develop a detailed model for a two-wheeled (i.e., two driving wheels) WMR that is one of the most commonly available WMRs using the above generalized formulation.

Ideal model: A WMR without wheel slip

The WMR shown in Fig. 3.3 is a standard platform of a nonholonomic two-wheeled mobile robot.

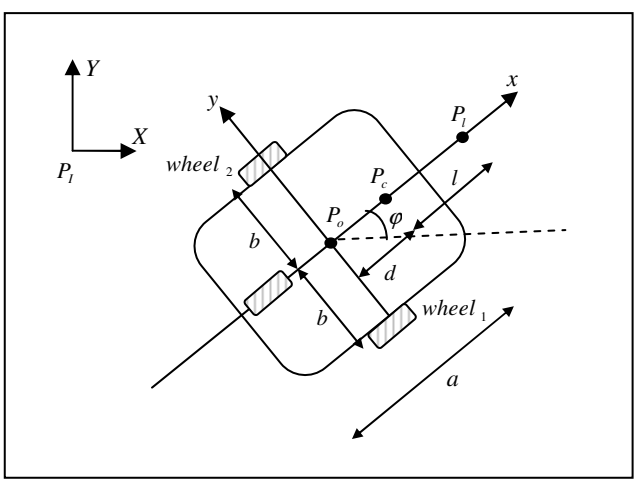

Fig. 3.3: A two-wheeled nonholonomic mobile robot platform

It has two differential-driving wheels and a castor wheel used for balancing. The differential driving wheels are from unicycle type as shown in Fig. 3.4. It has two degrees of freedom; the rotation around the motorized wheel axle and the contact point.

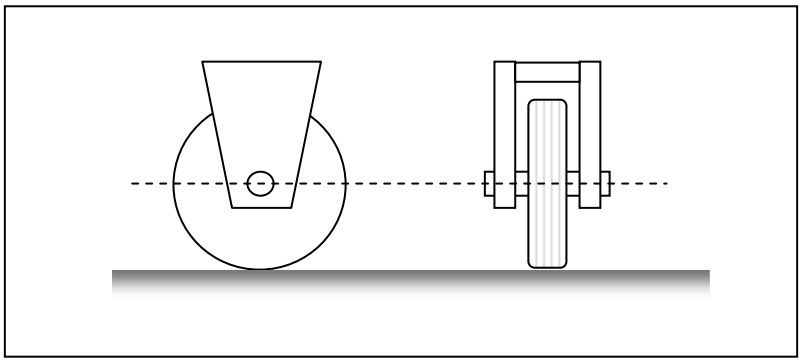

Fig. 3.4: A standard unicycle wheel

While the castor wheel as shown in Fig. 3.5 is located at the back of the WMR (i.e. can be located anywhere) and has three degrees of freedom which are the rotation around the wheel axle, the contact point and the castor wheel. In our wheel modeling, we assume all the wheels are deformable and rigidly held to the WMR platform.

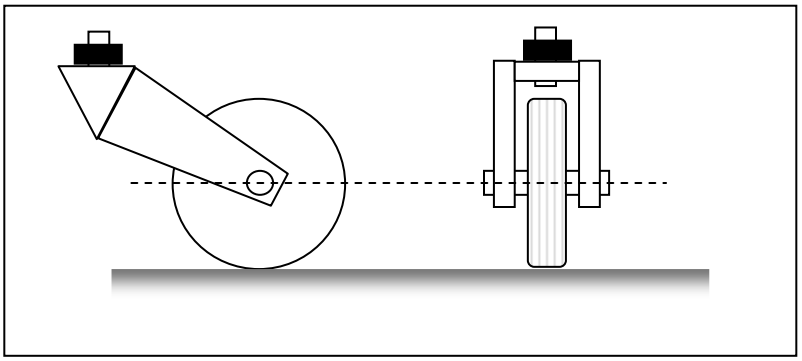

Fig. 3.5: A standard castor wheel

The two-driving wheels are powered by DC motors and have the same wheel radius, r. Point P_o is the origin of WMR axis, which is located at the intersection of the longitudinal x-axis and the lateral y-axis. The center of mass (COM) is located at point P_c. This point cannot be located at the intersection point of axis of symmetry of the platform, P_o to ensure no singularity in the control solution (Sarkar 1992, R. Zulli et. al. 1995). P_l is defined as a look-ahead point located on the x-axis of the WMR platform. b is the distance measured from the center of the WMR to the center of the wheel along the y-axis of the WMR reference frame. Here we assume the wheel model is represented by a thin, solid disk having a single point contact with the terrain surface. d denotes the distance between point P_o and point P_c along the x-axis. The distance of the look-ahead point is l from point P_c, which is also along the x-axis. The origin of the inertial frame $\{X,Y\}$ is shown as P_i and as such allows the pose of the WMR to be completely specified through the following vector of generalized coordinates,

$$q = [x_c, y_c, \varphi, \theta_1, \theta_2]^T \tag{3.15}$$

where x_c and y_c are the coordinate of the COM. φ represents the orientation of the WMR frame from the inertial frame and $[\theta_1, \theta_2]$ is the angular displacement vector for the WMR driving $wheel_1$ and $wheel_2$, respectively. Due to the nonholonomy of the system and by following the ideal no-slip assumption, the rolling constraints for both wheels are written as,

$$r\dot{\theta}_1 = \dot{x}_c \cos\varphi + \dot{y}_c \sin\varphi + b\dot{\varphi}$$

$$r\dot{\theta}_2 = \dot{x}_c \cos\varphi + \dot{y}_c \sin\varphi - b\dot{\varphi} \tag{3.16}$$

Eqn. (3.16) describes the longitudinal velocity of the WMR's center of mass that is constrained by the longitudinal velocity of the wheels generated due to pure rotation. By using the same premise, the knife-edge constraint can be written as follows,

$$0 = \dot{y}_c \cos\varphi - x_c \sin\varphi - d\dot{\varphi} \tag{3.17}$$

where the lateral velocity measured along the turning axis of the WMR is constrained to zero velocity. In order to derive the dynamic equation of the system using *Lagrangian* formalism, the WMR platform can be partitioned into three parts namely the body of the platform and its two wheels (i.e., $wheel_1, wheel_2$). The expression of the kinetic energy of the WMR body is given as,

$$T_r = \frac{1}{2} m_r (\dot{x}^2 + \dot{y}^2) + \frac{1}{2} I_{rz} \dot{\varphi}^2 \tag{3.18}$$

and the expression of the kinetic energy for both $wheel_1$ and $wheel_2$ are given respectively as,

$$T_{w1} = \frac{1}{2} m_w (\dot{x} + b\dot{\varphi}\cos\varphi + d\,\dot{\varphi}\sin\varphi)^2 + \frac{1}{2} m_w (\dot{y} + b\dot{\varphi}\sin\varphi - d\,\dot{\varphi}\cos\varphi)^2 + \frac{1}{2} I_{wz}\dot{\varphi}^2 + \frac{1}{2} I_{wy} \dot{\theta}_1{}^2 \tag{3.19}$$

$$T_{w2} = \frac{1}{2} m_w (\dot{x} - b\dot{\varphi}\cos\varphi + d\,\dot{\varphi}\sin\varphi)^2 + \frac{1}{2} m_w (\dot{y} - b\dot{\varphi}\sin\varphi - d\,\dot{\varphi}\cos\varphi)^2 + \frac{1}{2} I_{wz}\dot{\varphi}^2 + \frac{1}{2} I_{wy} \dot{\theta}_2{}^2 \tag{3.20}$$

By using the constraint equations (Eq. 3.16 and 3.17) and energy equations (Eq. 3.18-3.20), we can develop the dynamic equation for the WMR system without wheel slip as in the form of Eq. (3.6) or Eq. (3.14). The details of the derivation can be found in (Sarkar, Xiaoping & Kumar 1993).

In the next paragraph, we discuss the focus of this research, where the WMR is now subjected to wheel slip. For such a condition we basically relax the constraint equations and develop a new dynamic model of the WMR.

Non-ideal case: A WMR with wheel slips

In this research we want to investigate the navigation problem of a nonholonomic WMR when the ideal no-slip assumption does not hold true. In order to model that condition, we need to include slip into the dynamics of the system. We start by introducing the new set of generalized coordinates vector after no-slip condition is relaxed as follows,

$$q = [x_c, y_c, \varphi, \eta_1, \eta_2, \rho_1, \rho_2, \theta_1, \theta_2]^T \tag{3.21}$$

Note that, the slip-contributed states (i.e., ρ_i and η_i) can be easily expanded to accommodate a WMR with more fixed wheels. Using the new generalized coordinate vector, we can formulate the rolling constraints of the WMR with two fixed driving wheels in the following form,

$$\dot{\rho}_1 = \dot{x}_c \cos\varphi + \dot{y}_c \sin\varphi + b\dot{\varphi} \tag{3.22}$$

$$\dot{\rho}_2 = \dot{x}_c \cos\varphi + \dot{y}_c \sin\varphi - b\dot{\varphi} \tag{3.23}$$

where $\dot{\rho}_i = r\dot{\theta}_i - \dot{\zeta}_i$. The constraint equations, Eq. (3.22) and Eq. (3.23) relaxes the assumption of no-slip by allowing the longitudinal velocity at the wheel hub to be the summation of the longitudinal velocity generated by the wheel angular velocity, and the longitudinal slip velocity.

The same basis can be applied to develop the knife-edge/lateral constraints. Note that lateral slip in each wheel of a WMR is independent if the wheels are connected to the body of the WMR with mechanisms that allow relative motion (e.g., connected using springs and dampers). However, in our case as shown in Fig. 3.3, the two wheels of the WMR are rigidly connected to the body of the WMR and thus cannot have two different

lateral slips as can be seen from the following equations where both $\dot{\eta}_1$ and $\dot{\eta}_2$ have the same expressions,

$$\dot{\eta}_1 = \dot{y}_c \cos\varphi - x_c \sin\varphi - d\dot{\varphi} \tag{3.24}$$

$$\dot{\eta}_2 = \dot{y}_c \cos\varphi - x_c \sin\varphi - d\dot{\varphi} \tag{3.25}$$

where lateral slip is allowed to occur along the turning axis of the WMR during cornering. In this research, we analyze the effect of both slips, particularly, to investigate the agility of WMR navigation to negotiate sharp cornering. Now, after we rearrange the coordinate system, the new constraints defined above can be rewritten in the form of Eq. (3.4), where $A(q) \in \Re^{4\times 9}$ is given as follows,

$$A(q) = \begin{bmatrix} \cos\varphi & \sin\varphi & b & 0 & 0 & -1 & 0 & 0 & 0 \\ \cos\varphi & \sin\varphi & -b & 0 & 0 & 0 & -1 & 0 & 0 \\ -\sin\varphi & \cos\varphi & -d & -1 & 0 & 0 & 0 & 0 & 0 \\ -\sin\varphi & \cos\varphi & -d & 0 & -1 & 0 & 0 & 0 & 0 \end{bmatrix} \tag{3.26}$$

which is a full rank matrix. We can find matrix $S(q) \in \Re^{9\times 5}$ from $\mathcal{N}(A(q))$ to fulfill the requirement of Eq.(3.9) as,

$$S(q) = \begin{bmatrix} -\sin\varphi & \frac{(b\cos\varphi - d\sin\varphi)}{2b} & \frac{(b\cos\varphi + d\sin + d\sin\varphi)}{2b} & 0 & 0 \\ \cos\varphi & \frac{(d\cos\varphi + b\sin\varphi)}{2b} & \frac{(-d\cos\varphi + b\sin\varphi)}{2b} & 0 & 0 \\ 0 & \frac{1}{2b} & -\frac{1}{2b} & 0 & 0 \\ 1 & 0 & 0 & 0 & 0 \\ 1 & 0 & 0 & 0 & 0 \\ 0 & 1 & 0 & 0 & 0 \\ 0 & 0 & 1 & 0 & 0 \\ 0 & 0 & 0 & 1 & 0 \\ 0 & 0 & 0 & 0 & 1 \end{bmatrix} \tag{3.27}$$

In order to formulate the inertia matrix, we define the kinetic energy of the WMR as follows,

$$T_r = \frac{1}{2} m_r (\dot{x}^2 + \dot{y}^2) + \frac{1}{2} I_{rz} \dot{\varphi}^2 \tag{3.28}$$

$$T_{w1} = \frac{1}{2}m_w\left(\dot{\rho}_1{}^2\right) + \frac{1}{2}m_w\left(\dot{\eta}_1{}^2\right) + \frac{1}{2}I_{wz}\dot{\varphi}^2 + \frac{1}{2}I_{wy}\dot{\theta}_1{}^2 \tag{3.29}$$

$$T_{w2} = \frac{1}{2}m_w\left(\dot{\rho}_2{}^2\right) + \frac{1}{2}m_w\left(\dot{\eta}_2{}^2\right) + \frac{1}{2}I_{wz}\dot{\varphi}^2 + \frac{1}{2}I_{wy}\dot{\theta}_2{}^2 \tag{3.30}$$

where T_r is the kinetic energy of the WMR body and, T_{w1} and T_{w2} are the kinetic energies for $wheel_1$ and $wheel_2$, respectively. We found the inertia matrix, $M(q) \in \Re^{9\times 9}$ to be,

$$M = \begin{bmatrix} m_r & 0 & 0 & 0 & 0 & 0 & 0 & 0 & 0 \\ 0 & m_r & 0 & 0 & 0 & 0 & 0 & 0 & 0 \\ 0 & 0 & I_{rz} + 2I_{wz} & 0 & 0 & 0 & 0 & 0 & 0 \\ 0 & 0 & 0 & m_w & 0 & 0 & 0 & 0 & 0 \\ 0 & 0 & 0 & 0 & m_w & 0 & 0 & 0 & 0 \\ 0 & 0 & 0 & 0 & 0 & m_w & 0 & 0 & 0 \\ 0 & 0 & 0 & 0 & 0 & 0 & m_w & 0 & 0 \\ 0 & 0 & 0 & 0 & 0 & 0 & 0 & I_{wy} & 0 \\ 0 & 0 & 0 & 0 & 0 & 0 & 0 & 0 & I_{wy} \end{bmatrix} \tag{3.31}$$

which is positive definite and symmetric. We later introduce a vector of lateral traction force, f_{lat_i} and longitudinal traction force, f_{lon_i} as

$$F(\dot{q}) = [0,0,0, f_{lat1}, f_{lat2}, f_{lon1}, f_{lon2}, -rf_{lon1}, -rf_{lon2}]^T \tag{3.32}$$

where each individual element of the traction force vector is calculated from the magnitude of the respective slips. The dynamic equation of WMR system can now be represented as,

$$M(q)\ddot{q} = B(q)\tau + F(\dot{q}) + A^T\lambda \tag{3.33}$$

where the transformation matrix, $B(q)$ takes the form of,

$$B(q) = \begin{bmatrix} 0 & 0 & 0 & 0 & 0 & 0 & 0 & 1 & 0 \\ 0 & 0 & 0 & 0 & 0 & 0 & 0 & 0 & 1 \end{bmatrix}^T \tag{3.34}$$

The input τ is the torques to the driving wheels, given in the vector form,

$$\tau = \begin{bmatrix} \tau_1 \\ \tau_2 \end{bmatrix} \tag{3.35}$$

and the *Lagrange* multiplier,

$$\lambda = [\lambda_1 \quad \lambda_2 \quad \lambda_3 \quad \lambda_4]^T \tag{3.36}$$

We expand the dynamic equation, Eq. (3.33), to obtain the following set of equations,

$$m_r\ddot{x} = \cos\varphi\,(\lambda_1 + \lambda_2) - \sin\varphi\,(\lambda_3 + \lambda_4) \tag{3.37}$$

$$m_r\ddot{y} = \sin\varphi\,(\lambda_1 + \lambda_2) + \cos\varphi\,(\lambda_3 + \lambda_4) \tag{3.38}$$

$$(I_{rz} + 2I_{wz})\ddot{\varphi} = \mathrm{b}(\lambda_1 - \lambda_2) - \mathrm{d}(\lambda_3 + \lambda_4) \tag{3.39}$$

$$m_w\ddot{\eta}_1 = f_{lat1} - \lambda_3 \tag{3.40}$$

$$m_w\ddot{\eta}_2 = f_{lat2} - \lambda_4 \tag{3.41}$$

$$(I_{wy} + m_w r^2)\ddot{\theta}_1 = \tau_1 - r f_{lon1} \tag{3.44}$$

$$(I_{wy} + m_w r^2)\ddot{\theta}_2 = \tau_2 - r f_{lon2} \tag{3.45}$$

From these set of equations, we note that the last two equations (Eq. (3.44) and Eq. (3.45)) are independent of *Lagrange* multipliers, which are due to the constraint equations. This allow us to separate these two equations from the dynamic equation, Eq.(3.33), and eliminate the last two column of matrix $S(q)$, in Eq.(3.27). By following the procedure described in Eq. 3.4-3.14, we present the dynamics of the WMR in the following form,

$$\dot{\nu} = \begin{bmatrix} \ddot{\eta}_2 \\ \ddot{\rho}_1 \\ \ddot{\rho}_2 \end{bmatrix} = (S^T M S)^{-1} S^T\left(-M\dot{S}\nu\right) + (S^T M S)^{-1} S^T F = \varsigma + \kappa F \tag{3.46}$$

$$I_{wy}\ddot{\theta}_1 = \tau_1 - r f_{lon2} \tag{3.47}$$

$$I_{wy}\ddot{\theta}_2 = \tau_2 - r f_{lon2} \tag{3.48}$$

Derivation of the dynamic equation using Newton's method

Newton's method is another main formalism to derive the governing equation pertaining to the dynamics of a mechanical system. The *Newton* equations relate forces and torques to the linear and rotational accelerations of the body masses. In the following, we use Newton's method to rederive the dynamic equation of WMR to ensure the consistency of the model previously developed using Lagrange's method.

Using *free-body* approach, we isolate the WMR into three parts namely, the body of the WMR and its two wheels (i.e.,$wheel_1, wheel_2$), and account for all the forces and torques acting on the joints of the parts. Fig. 3.6 depicts the acting forces and torques on the parts using free body diagram.

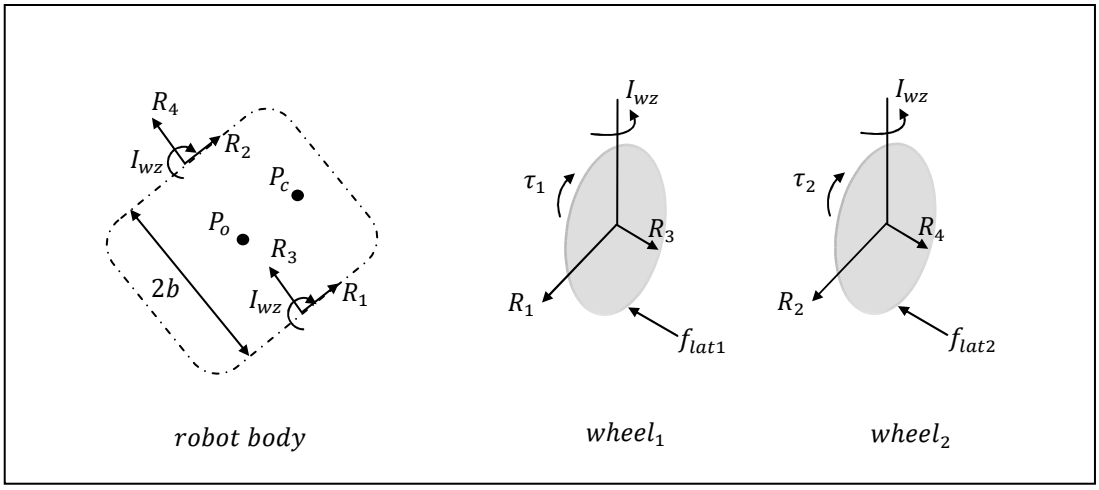

Fig. 3.6: Free body diagram of a wheeled-mobile robot

By letting R_i to be the reactive forces acting on the respective joints, the Newton equations for the body of the WMR are given as follows,

$$m_r\ddot{x} = \cos\varphi\,(R_1 + R_2) - \sin\varphi\,(R_3 + R_4) \tag{3.49}$$

$$m_r\ddot{y} = \sin\varphi\,(R_1 + R_2) + \cos\varphi\,(R_3 + R_4) \tag{3.50}$$

$$I_{rz}\ddot{\varphi} = \mathrm{b}(R_1 - R_2) - \mathrm{d}(R_3 + R_4) - 2I_{wz}\ddot{\varphi} \tag{3.51}$$

and for $wheel_1$ and $wheel_2$, the equations can be written as,

$$m_w\ddot{\eta}_1 = f_{lat1} - R_3 \tag{3.52}$$

$$m_w\ddot{\eta}_2 = f_{lat2} - R_4 \tag{3.53}$$

$$(I_{wy} + m_w r^2)\ddot{\theta}_1 = \tau_1 - rR_1 \tag{3.56}$$

$$(I_{wy} + m_w r^2)\ddot{\theta}_2 = \tau_2 - rR_2 \tag{3.57}$$

We observe the set of equations (Eq. 3.49-3.57) derived using Newton's method have the same form as the equations derived using Lagrange's method (Eq. 3.37-3.45) if we let the relationship between Lagrange's multipliers and the reactive forces to be,

$$R_i = \lambda_i \tag{3.58}$$

This shows the consistency between the two models developed using Newton's and Lagrange's methods. In the following chapter, we discuss the model of traction force and its relationship to wheel slips.

CHAPTER IV

WHEEL SLIP AND TRACTION FORCE

Increasing requirements on ride safety and comfort of vehicles inspired many research areas such as advanced vehicle control system, online system monitoring and wheel-surface (wheel-ground surface) traction force modeling. The latter involves the study on the mechanism to convert motor torque to traction force. The analysis of wheel-surface interaction can provide an insight into the understanding of vehicle dynamics so as to improve ride and trajectory performance. This is particularly important for an autonomous system like the WMR, where the control performance based on the model-based controller depends heavily on its dynamic model.

The main task of wheel-surface traction force modeling and monitoring is to determine the relationship between traction forces and slip velocity. However, the relationship is difficult to analyze due to the following three challenges. First, traction force is generated through tire deformation, tire adhesion as well as tire wear and tear, and it is influenced by several factors including wheel-surface conditions, tire pressure, and load etc. When there is a continuous interaction between the tire and the surface, the result is the elastic deformation at a molecular level of the outer layer of the tires called asperities shown in Fig. (4.1). The load of the WMR causes these asperities to penetrate the surface asperities. When this happens, it yields a resistance force or a traction force. Deformation of the tire provides most of the traction force. Adhesion is a property of the rubber that causes it to stick to other materials at the contact point. It is caused by the

molecular bonds between the rubber thread and the surface. The strength of the bonds relies on the temperature and the amount of slip occurs at the contact point. In addition to tire deformation and tire adhesion, the wear and tear of the wheel also contributes to the traction force.

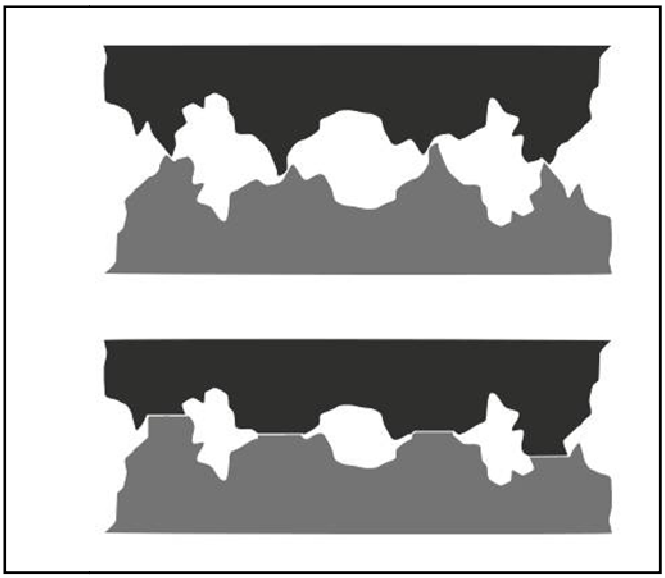

Fig. 4.1: Asperities deformation of two surfaces before load is applied (top) and after load is applied (bottom)

Second, the nonlinear and dynamic properties of traction force such as the viscous and hysteresis phenomenon are difficult to describe analytically. On the other hand, most empirical traction force models are hard to rationalize by physical laws.

Third, the complexity of the traction force model can affect the performance of the systems. For instance, for a system application, which is time critical, the model of the traction force should be able to be employed in real-time.

In this chapter, we describe the choice of traction force model used in this research. Our requirement is to have a traction model that is made up of a continuous, differentiable function.

Traction force models

The model of traction force can generally be classified into two types namely empirical (or semi-empirical) and analytical models. The former are developed based on curve-fitting techniques and can accurately capture the nonlinear characteristics of the traction force. However, most of these models lack physical interpretation, and cannot directly reflect the effects of some dynamic factors like tire hysteresis, humidity of the surface and tire pressure. Meanwhile, most analytical model of traction force is composed of differential equation. For example, *Brush* model can model the dynamic factors mentioned above (Li & Wang 2006). However, these models lack the empirical (semi-empirical) accuracy and as a result, the choice of the traction models greatly depends on the type of system applications. For a WMR that is equipped with standard unicycle wheels as described in Chapter III, the traction force acting on the longitudinal and lateral directions can be modeled separately, resulting in two independent traction force models, longitudinal and lateral traction models. Table 4.1 lists some of the most useful traction models found in the literatures.

Table 4.1: Traction force models and their brief descriptions

MODEL NAME	PROPERTIES	FEATURES
Piecewise Linear (longitudinal)	Empirical	Easy to identify but cannot accurately fit curves
Burckhardt model (longitudinal)	Semi-empirical	Can accurately fit curve
Rill model (longitudinal)	Semi-empirical	Easy to identify

Delft model or Magic formula (longitudinal and lateral)	Semi-empirical	Can accurately fit curves and model different factors
Dahl model (longitudinal)	Analytical	Can describe Coulomb friction and produce smooth transition around zero velocity
Bliman-Sorine (longitudinal)	Analytical	An improvement over Dahl's with an additional Stribeck effect
LuGre model (longitudinal)	Analytical	An improvement over Bliman-Sorine's with additional combination of pre-sliding and sliding factors
Linear Proportional (lateral)	Empirical	Cannot accurately reflect saturation properties but easy to identify
Nonlinear Proportional (lateral)	Semi-empirical	Can accurately fir curves
Bicycle (lateral)	Analytical	Does not reflect the traction force directly

The *Delft* model or famously known as *Magic formula* model is an elegant, semi-empirical model based on curve fitting. It has been widely accepted in the industry and academia (Politis et al. 2001, Li and Wang 2006) to generalize the model of both longitudinal and lateral traction forces. It was introduced by (Bakker, Nyborg & Pacejka 1987) and since then has been revised several times. The advantages of this model over the others stem from its accuracy, simplicity and ability to be interpreted. Due to these reasons, in this research we employ the *Magic formula* model of traction force. Moreover the model is composed of a continuous, differentiable function.

Slip (wheel slip) is a major component in the *Magic formula* model of traction force. It is an indirect measure of the fraction of the contact point that is sliding when the

velocity of the tire with respect to the surface at the contact patch is nonzero. In this dissertation, we define longitudinal slip as a slip that happened along the mean plane of the moving wheel and side slip as a slip that happens in lateral direction of a moving wheel. In the following we describe both types of slips under the framework of longitudinal and lateral traction force, respectively.

Longitudinal slip and longitudinal traction force

Longitudinal slip, $\dot{\zeta}$, also known as circumferential or tangential slip, happens along the mean plane of the wheel and is responsible for the generation of the longitudinal traction force. It is defined as a difference between the resultant linear velocity due to the angular velocity of the wheel, $r\dot{\theta}$, and the instantaneous velocity of the hub centerline of the wheel, V_{wx} with respect to the ground during acceleration and deceleration phases of motion. The term slip ratio, *sr*, is generally used to represent longitudinal slip and is defined as follows,

$$sr_i = \frac{r\dot{\theta}_i - V_{wx_i}}{max(r\dot{\theta}_i, V_{wx_i})} = \frac{\dot{\xi}_i}{max(r\dot{\theta}_i, V_{wx_i})} \tag{4.1}$$

where *i* denotes the *i*-th wheel. From Eq. (4.1), a free rolling wheel, where $V_{wx} = 0$ has the slip ratio, *sr* = 1 and for the wheel that rolls without slip, $V_{wx} = r\dot{\theta}$, the slip ratio, *sr* = 0. In this research we assume the wheel is rolling with slip. Thus, $V_{wx} = r\dot{\theta} - \dot{\xi}$ is an expression to represent the total longitudinal velocity of the WMR at the wheel hub centerline. In this research, the relationship between the longitudinal slip and the longitudinal traction force, f_{lon} in the *Magic formula* model of traction is presented as,

$$f_{lon} = Dsin\left(a_0 tan^{-1}\left(SB + E(tan^{-1}(SB) - SB)\right)\right) \tag{4.2}$$

where all the variables are given and described below,

$$\mu_{xp} = a_1 F_z + a_2 \tag{4.3}$$

$$D = \mu_{xp} F_z \tag{4.4}$$

$$Ba_0 D = (a_3 F_z^2 + a_4 F_z)e^{-a5Fz} \tag{4.5}$$

$$E = a_6 F_z^2 + a_7 F_z + a_8 \tag{4.6}$$

$$S = 100sr + a_9 F_z + a_{10} \tag{4.7}$$

F_z is the weight of the WMR in kN and the eleven empirical numbers, a_i , $i \in \{1,2,\dots,11\}$, are used to characterize a particular tire. Eq. (4.3) is a linear function of weight that estimates the peak of longitudinal friction coefficient. In Eq. (4.4), we see D as a linear function of F_z, where μ_{xp} can be treated as a regular coefficient of traction function and a_2 in Eq. (4.3) can be seen as a direct measurement of the degree of tire stickiness. B in Eq. (4.5) scales the other independent variable, $a_0 D$ and is known as a stiffness factor. Eq. (4.6) represents E as a factor known as the curvature factor. It determines the shape around the peak of the curve. The last variable, S in Eq. (4.7) is a function of slip ratio, sr which can be measured directly from the system. Fig. 4.2 shows some examples of longitudinal traction force or longitudinal traction curve for rubber wheel for different type of surfaces. A region on the left of the peak force starts linearly and is known as a stable region. Increasing the slip ratio passing the peak force will significantly decreases the traction force and thus the whole region on the right of the peak force should be avoided as it represents instability.

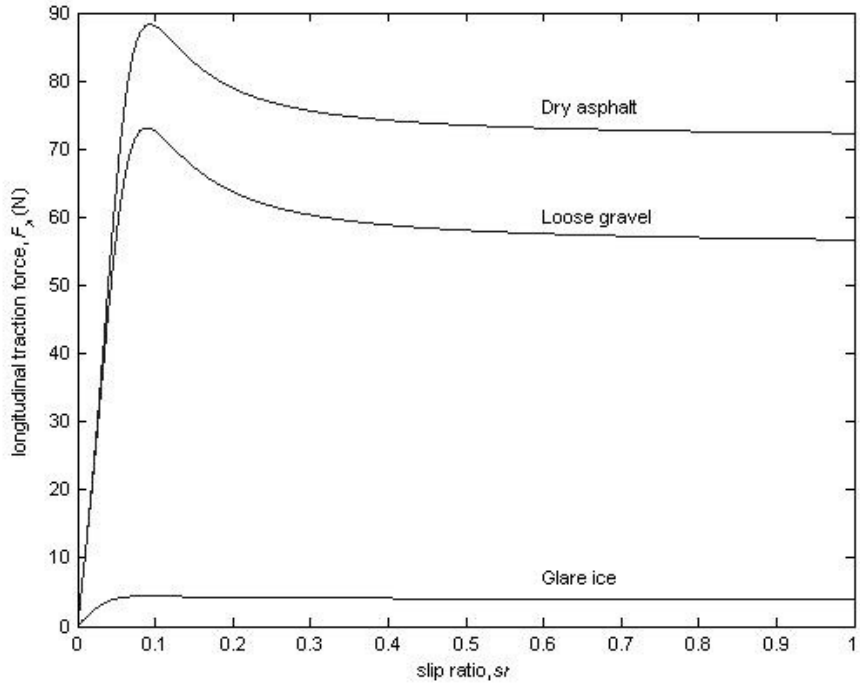

Fig. 4.2: Some examples of traction curves for a variety of surface types

Lateral slip and lateral traction force

Lateral traction force, f_{lat}, is generated as a result of slip angle, *sa*, during wheel cornering. It is sometimes known as cornering force. Slip angle is defined as the angle between the instantaneous velocity of the WMR and the instantaneous linear velocity of the wheel. In this research this term is defined as follows,

$$sa_i = tan^{-1}\left(\frac{\dot{\eta}_i}{\dot{\rho}_i}\right) \tag{4.8}$$

where $\dot{\eta}_i$ is the lateral slip of the *i*-th wheel and $\rho_i = r\theta_i - \zeta_i$ is total longitudinal displacement of the *i*-th wheel. The *Magic formula* model to define lateral force is almost identical to its longitudinal counterpart but requires significantly different interpretation.

Besides *sa*, there are fifteen more empirical numbers, b_i , $i \in \{1,2,\dots,15\}$ that help to construct the lateral traction model, which can be written as follows,

$$F_z = Dsin\left(b_0 tan^{-1}\left(SB + E(tan^{-1}(SB) - SB)\right)\right) + s_v \tag{4.9}$$

where the variables and their brief descriptions are given below.

$$\mu_{yp} = b_1 F_z + b_2 \tag{4.10}$$

$$D = \mu_{yp} F_z \tag{4.11}$$

$$Ba_0 D = b_3 sin\left(2tan^{-1}(F_z/b_4)\right)(1 - b_5|\gamma|) \tag{4.12}$$

$$S = sa + b_8\gamma + b_9 F_z + b_{10} \tag{4.13}$$

$$E = b_6 F_z + b_7 \tag{4.14}$$

$$S_v = \left((b_{11}F_z + b_{12})\gamma + b_{13}\right)F_z + b_{14} \tag{4.15}$$

Eq. (4.10) defines the peak of lateral friction coefficient. The variable, *D*, in Eq. (4.11) defines the product of the friction coefficient and the normal force, F_z. In general, the term b_2 in the equation must be significantly larger than $b_1 F_z$ to maintain the Newtonian behavior of the traction force. The variable *B* given in Eq. (4.12) has different interpretation where γ is the camber angle of the wheel measured in degree. The fourth variable in Eq. (4.13) and the last variable in Eq. (4.14) can be measured in a straight forward manner. In addition to the above-mentioned variables, the lateral traction form of *Magic formula* requires an additive correction term for *ply steer* and *conicity*, (Eq. (4.15)). Fig. (4.3) shows a plot of lateral traction force or also know as traction curve for different surfaces with different friction coefficient (Pasterkamp 1997).

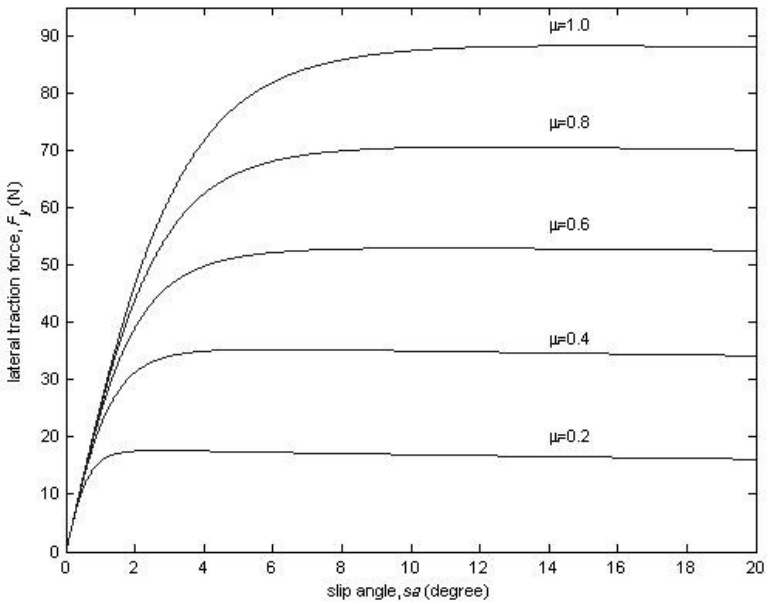

Fig. 4.3: Some examples of lateral traction curves for a variety of surfaces with different friction coefficients

CHAPTER V

WMR MODEL VERIFICATION

Designing new planners and controllers for the WMR through experimentation can be hazardous as well as costly in terms of time and resources. Realistic simulation can be an attractive alternative to the real experiments. If we are able to develop a realistic WMR model, predictions regarding the output of the real experiments could be made from the simulation study. It allows systematic analysis of the WMR dynamic behavior and provides fast and flexible development of new planners and controllers for the WMR. (Nehmzow 2003) quotes the computer simulation as,

"model which is amenable to manipulations which would be impossible, too expensive or impractical to perform on the entity it portrays. The operation of the model can be studied and, from it, properties concerning the behavior of the actual system or its subsystems can be inferred."

The basic requirement of a realistic WMR simulation implies the existence of a reliable model of the system. The majority of the on-shelf wheeled mobile robot platforms available, such as *Robulab*, *Roburoc* (URL 5.1), *Trilobot Research Robot* (URL 5.2), and *Pioneer*, *AmigoBot* and *PowerBot* (URL 5.3) come with their own simulator software (i.e. *MobileSim for Pioneer robot*). Additionally, a number of more general purpose WMR simulators have also been developed based on the open-source platform, which allows wider access to multiple WMR platforms such as *Stage* and *OpenSim*. While majority of the WMR simulators have become quite useful for general WMR

applications, they do not model wheel slip and thus may not be able to describe the robot behavior correctly and effectively where wheel slip is a critical factor (URL 1.10). At low speed, these WMR models may be valid but when the slip is significant the navigation and control algorithms develop based on these models may result in undesirable performance.

In this chapter, we present the verification of the WMR model developed in Chapter III through a series of experimental studies. In particular, we want to investigate the dynamics of the WMR while taking a sharp turn at high speed and when asked to move along a straight line on slippery surface.

WMR motion task: sharp cornering at high speed

One of the reasons to have high speed navigation for a WMR is to achieve service efficiencies. However, there are fundamental difficulties when we want to increase the speed of a WMR. (**Chung, Kim, & Choi. May 2006**) classified the difficulties into three categories: i) unexpected dynamic changes of the environment likes the abrupt appearance of obstacles; ii) the control and computational limitations due to the system response for real time applications; and iii) the dynamic and mechanical limitations.

In this chapter, we first discuss the dynamics of the WMR during sharp cornering at high speed when the lateral velocities are generated and the wheel side slip, $\dot{\eta}$, could become large enough to impact the overall performance of the system (Travis, Bevly 2005). Here the term high speed is a relative concept and is defined with respect to the surface on which the WMR is traversing. For example, for the WMR under study we

define high speed to be 0.8*m/s* when the WMR is traversing on the slippery surface (it may not be the case if the surface has higher traction such as a dry pavement).

Simulation parameters

In the model simulation, our objective is to observe the dynamics of the WMR that is asked to follow an *L*-shape path (i.e., a sharp corner) in an open-loop manner with torque as the input to both wheels. The simulated model is based on *Pioneer P3DX* (two wheeled mobile robot) manufactured by *MobileRobot Inc.* shown in Fig. 5.1 and can be represented schematically as in Fig. 3.3.

Fig. 5.1: *Pioneer P3DX*, the two wheeled mobile robot platform

We employ Eq. (3.33) to model the dynamics of the *Pioneer PD3X* WMR and set the WMR parameters (refer Fig. 3.3) as follows: $b = 0.24m$; $d = 0.05m$; $r = 0.095$; $m_r = 17kg$; $m_w = 0.5kg$; $I_{rz} = 0.537kgm^2$; $I_{wy} = 0.0023kgm^2$; $I_{rz} = 0.0011kgm^2$. The respective moment of inertia values are obtained by assuming the WMR body to take a solid cuboid shape of *height* x *width* x *length* = 0.245*m* x 0.4*m* x 0.45*m* and each wheel to be of the form of a thin, solid disk of radius, *r* and mass, m_w.

Experimental setup

The goal of the experiment is to replicate the results obtained from the simulation studies as best as possible in order to verify the WMR analytical model developed for this research. For a particular *Pioneer P3DX* WMR platform, the lack of lateral velocity sensing unit requires us to select a proper sensor to measure the quantity. We opt for an accelerometer, *MDS302,* manufactured by *Mechworks System Inc.* as shown in Fig. 5.2.

Fig. 5.2: Accelerometer, *MDS302*

The accelerometer can read up to ±2*g* acceleration, which is suitable for our WMR application. We found that on a planar surface, the choice of using accelerometer is sufficient to measure the lateral slip in order to validate our dynamic model. We also realize that, by using direct integration method to find lateral slip measurement from accelerometer signal is prone to 'drift' problem. However, with proper adjustment of the offset value we are able to minimize this problem. The availability of an extra serial port on the *Pioneer P3DX* allows this external accelerometer to be directly tethered and positioned on the system as shown in Fig. 5.1.

We program the accelerometer to run along the program of the *Pioneer P3DX* in synchronous mode where several tasks are done in multithread with proper prioritization.

(the sample program can be found in the Appendix). The data from each task are updated for every 100*ms* of robot command cycle. As a result, the processing of accelerometer signal (i.e., filtering, data conversion) into velocity during each command cycle limits the sampling rate of the accelerometer data to 10*samples/s* from each axis. The faster sampling rate used, causes delay and overflow in the system buffer and the slower sampling rate, lessens the signal resolution. We reduce the effect of noise by applying a built-in 5th order Butterworth filter with cut off frequency of 50*Hz*.

Sharp cornering motion through open loop control: results and discussion

We run the simulation studies and the experiments to investigate the *Pioneer P3DX* dynamics using the open loop control. The idea to apply the open loop control is to provide a common platform for the simulated dynamic model of the *Pioneer P3DX* to be compared to the real *Pioneer P3DX* and to isolate any input that exists in the feedforward/feedback control approach. With regard to this point, we consider the closed loop response of the low-level built-in PID controller in the *Pioneer P3DX* to have insignificant impact especially on the overall, qualitative performance of the system.

In our studies, the *Pioneer P3DX* is commanded to move on two surfaces:

Surface 1: a clean tiled surface (non-slippery)

Surface 2: a powder-layered tiled surface (slippery)

In order to identify the friction coefficient between the wheel (i.e., tire) of the *Pioneer P3DX* and these surfaces, we conduct a simple experiment to measure the friction coefficient of these surfaces. Fig. 5.3 shows the surfaces we conduct the experiment on and Fig. 5.4 displays the type of tire the *Pioneer P3DX* is equipped with.

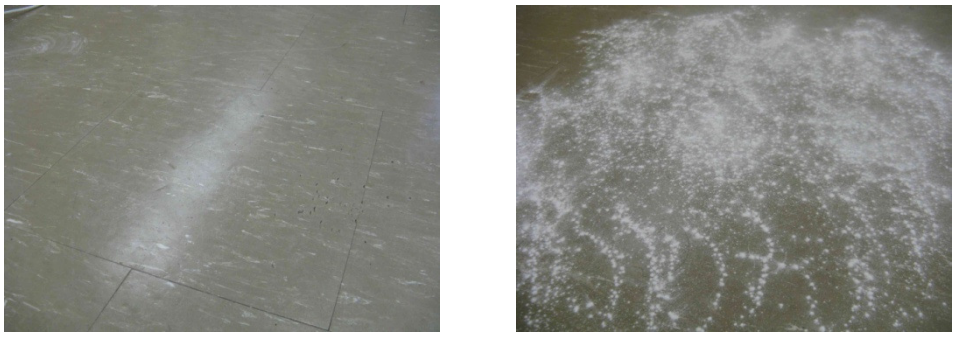

(a) (b)

Fig.5.3: Type of surfaces, (a): clean tiled surface (non-slippery), (b): powder-layered tiled surface (slippery)

(a) (b)

Fig.5.4: (a): Wheel of *Pioneer P3DX* (b): Tire thread

In Fig. 5.5, we show the experiment set-up. The electronic scale, acting as a dynamometer is hooked up to one end of the robot.

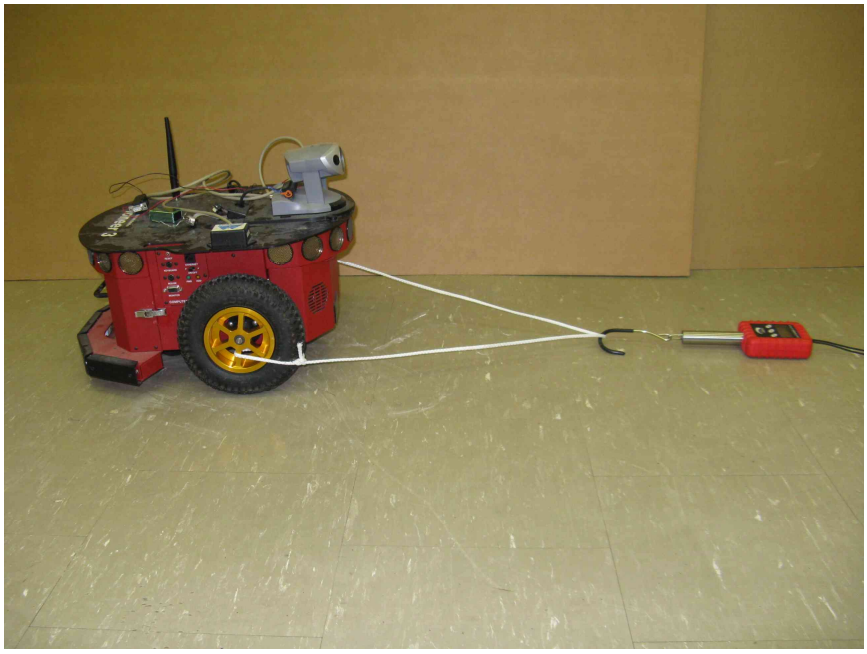

Fig. 5.5: Experimental setup to measure friction coefficient, μ_d

We pull the robot using the dynamometer and once the wheels start to slip, we continuously pull the dynamometer at constant speed and record the measurement. We run the experiment at random locations around the surface area so as to capture as much variations in the value of friction coefficient for that surface. Table 5.1 and 5.2 show the measurement of longitudinal and lateral traction forces data respectively, where for each surface we take 10 samples of data.

Table 5.1: Data of longitudinal traction force measurement

Longitudinal traction force on non-slippery surface (*kgf*)	Longitudinal traction force on slippery surface (*kgf*)
11.45	4.90
11.19	5.03
10.43	4.60
9.19	4.79
10.96	5.60

9.20	5.00
12.50	5.17
11.79	5.30
10.62	4.80
12.60	5.40
F_{ave} =10.993	F_{ave}=5.095

Table 5.2: Data of lateral traction force measurement

Lateral traction force on non-slippery surface (*kgf*)	Lateral traction force on slippery surface (*kgf*)
6.27	3.82
6.50	3.89
6.80	4.02
6.02	4.32
7.90	4.19
7.63	3.97
6.59	3.85
7.66	4.50
7.95	4.31
7.38	4.22
F_{ave} =6.941	F_{ave}=4.109

The *Pioneer P3DX* weighs 18kg and to estimate the value of longitudinal and lateral friction coefficients, μ_{dlon} and μ_{dlat} , we use the following equation,

$$F_{ave} = \mu_d m_{WMR} g \tag{5.1}$$

where m_{WMR} is the weight of the WMR, g is the gravitational acceleration and μ_d is μ_{dlon} for longitudinal case and μ_{dlat} for lateral case. We find μ_{dlon} and μ_{dlat} for the non-slippery surface to be 0.6107 and 0.3856 respectively, and for the slippery surface to be 0.2811 and 0.2283.

In order to study the effect of slip in sharp cornering motion, we command the WMR to start turning at a reference point (i.e., the point that connects two straight segments to form an *L*-shaped path). Fig. 5.6(a) shows the resultant trajectory of the

Pioneer P3DX on the clean, tiled surface (non-slippery surface). We find the trajectory is stable with negligible lateral slip and the *Pioneer P3DX* is able to respond to sharp cornering command satisfactory by moving parallel to the second straight segment of the path with insignificant deviation. Similar trajectory is also produced from the standard *Pioneer* simulator (i.e., *MobileSim 3.0*) shown in Fig. 5.6(b). (Note: The *MobileSim* produces small deviation from the *L*-shaped path, due to the strict 100*ms* robot command cycle, the program has to obey. However this is not the case for the real system where the command cycle can be from 90*ms* to 110*ms* resulted in the consistent *L*-shape trajectory for non-slippery surface). In Fig. 5.6(c), we present the result of the *Pioneer P3DX* simulation based on the new dynamic model where the surface is not slippery (i.e., the surface provides high traction). The trajectory of this model matches the real trajectory of the WMR when taking a sharp corner. Here, the magnitude of the lateral slip is shown to be relatively small as discussed later. In this experiment, we set the longitudinal friction coefficient μ_{dlon} and the lateral friction coefficient μ_{dlat} to be 0.6107 and 0.3856 respectively.

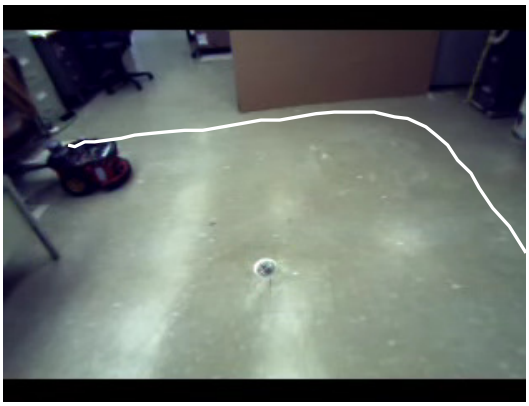

(a)

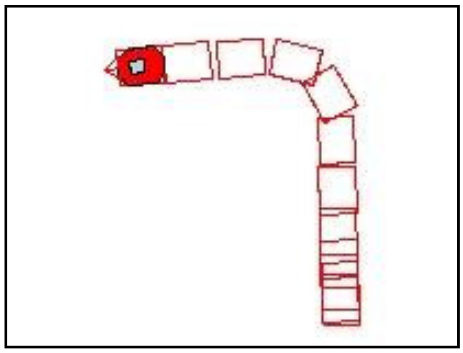

(b)

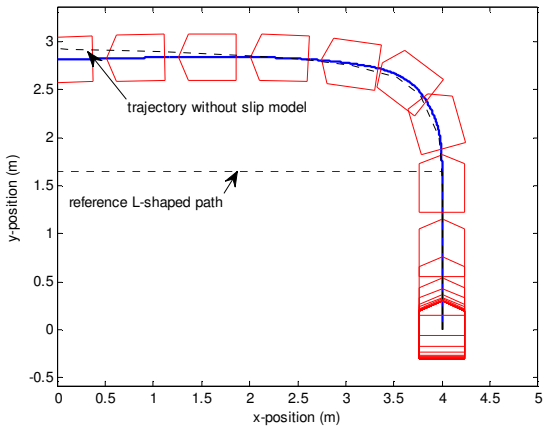

(c)

Fig.5.6: Trajectories of Pioneer P3DX on surface with negligible slip (a): experiment, (b): standard simulator model, (c): new dynamic model